Fuel 362 (2024) 130811

Contents lists available at ScienceDirect

Fuel

journal homepage: www.elsevier.com/locate/fuel

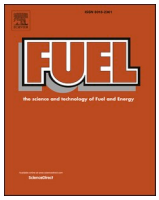

Full Length Article

Syngas-Enriched hydrogen production via catalytic gasification of water hyacinth using renewable palm kernel shell hydrochar

April Ling Kwang Chee [a], Bridgid Lai Fui Chin [a,b,*], Shaharin Anwar Sulaiman [c], Yee Ho Chai [d,e], Agus Saptoro [a,f], Hadiza Aminu Umar [c,g], Serene Sow Mun Lock [h], Chung Long Yiin [i,j]

[a] Department of Chemical and Energy Engineering, Faculty of Engineering and Science, Curtin University Malaysia, CDT250, 98009 Miri, Sarawak, Malaysia
[b] Energy and Environment Research Cluster, Faculty of Engineering and Science, Curtin University Malaysia, CDT 250, 98009 Miri, Sarawak, Malaysia
[c] Department of Mechanical Engineering, Universiti Teknologi PETRONAS (UTP), 32610 Seri Iskandar, Perak Darul Ridzuan, Malaysia
[d] Chemical Engineering Department, Universiti Teknologi PETRONAS (UTP), 32610 Seri Iskandar, Perak Darul Ridzuan, Malaysia
[e] HICoE-Centre for Biofuel and Biochemical Research, Institute of Self-Sustainable Building, Universiti Teknologi PETRONAS (UTP), 32610 Seri Iskandar, Perak Darul Ridzuan, Malaysia
[f] Curtin Malaysia Research Institute (CMRI), Curtin University Malaysia, CDT250, 98009 Miri, Sarawak, Malaysia
[g] Mechanical Engineering Department, Bayero University Kano, PMB 3011, Kano, Nigeria
[h] CO_2 Research Center (CO_2RES), Department of Chemical Engineering, Universiti Teknologi PETRONAS (UTP), 32610 Seri Iskandar, Malaysia
[i] Department of Chemical Engineering and Energy Sustainability, Faculty of Engineering, Universiti Malaysia Sarawak (UNIMAS), 94300 Kota Samarahan, Sarawak, Malaysia
[j] Institute of Sustainable and Renewable Energy (ISuRE), Universiti Malaysia Sarawak (UNIMAS), 94300 Kota Samarahan, Sarawak, Malaysia

ARTICLE INFO

Keywords:
Water hyacinth
Syngas
Catalytic gasification
Hydrochar
Downdraft gasifier

ABSTRACT

Syngas produced from biomass gasification has emerged as a highly promising substitute for conventional fossil fuel, catering to various industrial applications while ensuring minimal greenhouse gas emissions. Water hyacinth (WH) has been a major concern due to its invasive nature and uncontrollable growth which impedes aquatic growth and urban management. Fortunately, WH is a potential biomass feedstock due to the comparable cellulose and hemicellulose contents alongside high carbon content and high calorific value which reflects good biofuel properties. Therefore, this study aims to investigate the conversion of WH biomass via catalytic air gasification for syngas-enriched hydrogen production using palm kernel shell hydrochar (PKSH). A parametric study was conducted in a lab-scale fixed-bed downdraft gasifier based on the response surface methodology coupled with Box-Behnken design (RSM-BBD). The combined interaction effects of the influencing parameters investigated are temperature (600–800 °C), biomass particle size (2–6 mm), catalyst loading (0–10 wt%), and air flow rate (1–3 L/min). Temperature was revealed to be the primary factor with significant influence on the H_2 and CO output. Maximum syngas (30.09 vol%) compositions of 11.14 vol% H_2 and 18.95 vol% CO were obtained at 800 °C with a particle size of 6 mm and air flow rate of 2 L/min alongside 5 wt% PKSH catalyst loading.

1. Introduction

The rapidly surging population implies high demand for resources and energy which places a downward pressure on the resources available. Consequently, various technologies and mitigation approaches arise to manage and enhance current resource utilization. Various alternative technologies and energy sources have been developed to aid the paradigm shift from conventional resources to sustainable and renewable energy sources. Thermochemical conversion of biomass into biofuels has garnered huge interest in recent years due to the attractive characteristic of biomass being carbon neutral nature, which leaves minimal to no carbon footprint while meeting the ever-increasing energy demand on a global basis [1–3]. Furthermore, thermochemical conversion, regarded as a promising viable approach for carbon monoxide (CO_2) mitigation, provides better conversion rate, flexibility, and robustness than the other conversion methods [4]. Biomass originating from the aquaculture sector is one to consider for biomass conversion into value-added products. Table 1 below summarizes recent studies on pyrolysis and gasification of aquatic plants in the past 5 years.

The aquatic weed, water hyacinth (*Pontederia crassipes*), is deemed as

* Corresponding author.
E-mail addresses: bridgidchin@curtin.edu.my, bridgidchin@gmail.com (B.L.F. Chin).

https://doi.org/10.1016/j.fuel.2023.130811
Received 1 August 2023; Received in revised form 10 December 2023; Accepted 28 December 2023
Available online 6 January 2024

Table 1
Summary of conversion of aquatic plants via pyrolysis and gasification methods.

Aquatic plants	Operating conditions	Gas yield	References
Micro-algae *Chlorella vulgaris* (CV) and *spirulina* (SP)	Air gasification Temperature: 30–800 °C Heating rate: 10–30 °C/min Gas flow rate: 500 ml/min (20 %O_2:80 %Ar) Pressure: 1 atm	**CV:** H_2 ~ 500 ml/g; CO ~ 400 ml/g; CO_2 ~ 400 ml/g; CH_4 ~ 80 ml/g **SP:** H_2 ~ 150 ml/g; CO ~ 230 ml/g; CO_2 ~ 500 ml/g; CH_4 ~ 30 ml/g	[5]
Seaweed	Fast pyrolysis Temperature: 25–700 °C Heating rate: 10–40 °C/min Argon (Ar) flow rate: 100 ml/min	~17 %	[6]
Water hyacinth	Pyrolysis Temperature: 250–550 °C Heating rate: 30–50 °C/min N_2 flow rate: 33.33–666.67 cm^3/min Particle size: 0.15–2 mm	25–42 wt%	[7]
Water hyacinth	Catalytic pyrolysis Temperature: 540 °C Heating rate: 25 min/°C N_2 flow rate: 35 ml/min Catalyst: 2 M $FeCl_3{\cdot}6H_2O$	278 ml/g H_2 – 42 %; CO_2 – 23 %; CO – 22 %; CH_4 – 7 %	[8]
Alligator weed	Catalytic pyrolysis Temperature: 450 °C Heating rate: 50 min/°C N_2 flow rate: 0.2 L/min Catalyst: $SnCl_2$, $Al_2O_3.4SiO_2{\cdot}H_2O$, MoS_2	H_2 – 12 mol%; CO – 26 mol%	[9]

a promising feedstock for energy recovery via thermochemical conversion as it was found to possess relatively high carbon content (33.33–42.90 wt%) and hydrogen content (5.69–6.27 wt%), alongside with high calorific value (13.59–17.39 MJ/kg) [10,11,7]. Water hyacinth (WH) originated from tropical South America and has been introduced worldwide as an ornamental plant due to its distinctive purple flower. This aquatic plant was also utilized as a biological treatment of shellfish wastewater (i.e., shrimp farming), particularly for removing pollutants [12]. However, a major downside of WH is its rapid reproduction rate of 220 kg per hectare per day [13]. Some of the challenges brought by the existence of WH include interference with navigation and irrigation systems as well as power generation and fishery schemes. The proliferation of WH has made it essential to convert such aquatic weeds into value-added products by harnessing their green energy, hence achieving sustainable and clean renewable energy. Of the various thermochemical conversions available, pyrolysis was predominantly the main conversion route for WH biomass in previous studies [10,14,15,8]. While biomass gasification has been a prominent approach, very limited studies were reported on the utilization of WH for syngas production despite its high carbon content and calorific value. Gasification stands out among the other thermochemical conversions for syngas production as it can convert biomass into syngas with low net CO_2 emissions. Syngas, primarily hydrogen (H_2) and carbon monoxide (CO), is particularly useful for electricity generation and could serve as feedstock for producing a wide range of fuel and chemicals. Furthermore, supercritical water gasification of WH offered better conversion and energy efficiency at 64.9 %, compared to bio-methanation at 49.3 % [16].

Extensive research has been carried out to explore new possible catalysts for biomass gasification. Renewable catalysts such as char could be the potential direction as a catalyst source. Char is typically produced as a by-product from the thermochemical conversion of biomass. It possesses high specific surface area, unique porous structure, and functional groups, making it an ideal catalyst that can be obtained at low cost and yet with high reliability [17]. It was reported that activated biochar derived from hardwood pyrolysis was effective in tar removal at 650–750 °C whereby its mesoporous and microporous structure induced high tar conversion [18]. An alternative form of char, such as hydrochar produced from hydrothermal carbonization (HTC) as a pre-treatment precursor, was reported to have enhanced its stability and textural properties, allowing it to be a viable catalyst support with its stable mesoporous structure [19–21]. Such hydrochar is rich in oxygenated functional groups such as carbonyl, carboxyl, and hydroxyl, which were reported to have provided significant effect on the carbon–metal precursor interaction for enhanced catalytic ability in gasification process [21]. Char catalysts were reported to have shown effective tar reduction and better yield and selectivity towards the final product distribution [19]. It is worth noting that the catalytic activity of char catalysts is comparable to that of dolomite [22]. The presence of inorganic elements, the alkali and alkaline earth metals (AAEM) is deemed to have further promoted the catalytic effect which enhances biomass gasification [23]. Using char as catalysts would aid in achieving a circular economy while creating an opportunity for the widespread use of biocatalysts, thereby reducing its price and enabling sustainable production.

Nonetheless, no study was reported on the catalytic gasification of WH biomass. It is observed that there had yet to be a study involving the combined interaction effect of parameters on the gaseous output (H_2, CO, CO_2, CH_4) from catalytic gasification of WH. Therefore, the current study aims to investigate the catalytic gasification of WH for syngas enriched hydrogen production using a renewable catalyst PKSH in a downdraft gasifier. The experimental design was conducted using RSM-BBD. RSM-BBD is a new optimization technique that has been proven effective in several gasification studies [24–26] as it allows the correlations between the input and output variables to be established, which aids the prediction of gaseous output at certain parameter configurations. As an effective multivariate technique, BBD features a rotatable design that offers a comparatively steady distribution of scaled prediction variance for the experimental design [27]. Furthermore, BBD allows fewer runs for optimization study which aids in conserving resources and expenses [28].

2. Methodology

2.1. Material preparation

WH was collected from the lake of Curtin University, Malaysia, and dried for four consecutive sunny days (48 h under the sun) before further drying in an oven at 105 °C for 4 h. This ensures moisture content was kept below 30 wt% [29–31]. Dried WH was grounded and sieved to different particle sizes (250 μm for characterization; 2 mm, 4 mm, and 6 mm for gasification). Proximate analysis was performed in a thermogravimetric analyzer (TGA/DSC 3+, Mettler Toledo), ultimate analysis in a CHNS analyzer (Vario MICRO, Elementar) and a bomb calorimeter (IKA C2000, Isoperibol) was used for calorific value analysis. The characterization tests were conducted as per ASTM D7582-12, ASTM D3176-09 and ASTM D4809-18 standards, respectively. Table 2 represents the characterization results. The detailed preparation of PKSH can be found under Section S1 in Supplementary Material.

2.2. Catalyst characterization

Elemental composition of the hydrochar was done via X-ray fluorescence (XRF) analysis in which the composition was measured using the XRF Bruker S8 Tiger machine. Field-emission scanning electron microscopy-energy dispersive X-ray (FESEM-EDX) analysis was conducted using Zeiss Supra 55 VP model machine to obtain the surface morphology images and mapping of the feedstock and catalysts at a magnification of 10,000x.

Table 2
Characterization of WH, PKS, and PKSH.

Sample	WH	PKS	PKSH
Proximate analysis, dry mass fraction basis (wt.%)			
Moisture	15.39	9.02	6.21
Volatile matter	76.27	66.99	57.13
Fixed carbon	3.47	19.94	29.79
Ash	4.87	4.05	6.87
Ultimate analysis, dry ash basis (wt.%)			
Carbon, C	32.01	49.36	57.73
Hydrogen, H	5.37	6.05	5.17
Nitrogen, N	3.16	2.88	2.98
Sulphur, S	0.21	0.06	0.07
Oxygen, O [a]	59.25	41.66	34.05
Calorific value (MJ/kg)	15.20	18.61	–

[a] By difference.

2.3. Experimental setup and procedure for catalytic gasification

Gasification of WH was conducted in a lab-scale gasifier that functions in allothermal mode. Fig. 1. represents the schematic diagram of a gasification system setup.

The gasifier comprises a vertical cylindrical casing (750 mm height, and 67 mm internal diameter) placed within a ceramic electric heater of 1.25 kW. Cleaning has to be done prior to the batch feeding (50 g) at each experimental run. Batch feeding was done by removing the lid of the gasifier from the top to pour the biomass feedstock into the gasifier and the lid was swiftly closed. The temperature microcontroller employs a Type-K thermocouple for temperature adjustment. The target gasification temperature ranges from 600 °C to 800 °C. The air compressor attached to the gasifier functions as an air supply and is regulated by a rotameter. The range of air flow rate supplied to the gasifier was between 1 L/min and 3 L/min. During gasification, gaseous products leave through the bottom of the gasifier and flow through a tube connected to the cooling and filtering unit before entering the gas analyzer (X-STREAM X2GP model). A ceramic filter of 4.0 μm in the unit filters particulate matter in the gas sample before flowing into the gas analyzer which displays the information on the gas compositions in terms of volume percentage readings.

2.4. Design of experiment

The parametric study of catalytic air gasification of WH was designed using RSM in Design-Expert 13 software. A computer-aided based software approach is applied because it allows the combined interaction effect of variables to be examined easily while the traditional experimental method entails manipulating one factor at a time which would be tedious to carry out and to process a large amount of data. BBD is selected as the design type for present study because BBD allows fewer runs and thereby conserving expenses and resources, allowing an efficient optimization process [25]. The range of the four influencing parameters to be assessed, such as temperature varies from 600 °C to 800 °C, biomass particle size from 2 to 6 mm, catalyst loading from 0 to 10 wt% and air flow rate from 1 L/min to 3 L/min. The effect of the parameters on the response variables, namely CO (vol.%), CO_2 (vol.%), CH_4 (vol.%) and H_2 (vol.%), will be observed. The experimental array consists of 29 experimental runs, inclusive of five central runs while the remaining are factorial runs. Table 3 represents the three levels of each input variable. Analysis of variance (ANOVA) was conducted after obtaining the experimental results to identify the interaction correlation between the input variables.

ANOVA allows the regression model to be examined as a whole and evaluates the individual and interactive impacts. A quadratic model was employed for the analysis where empirical equations were developed to demonstrate the correlation between the input factors and response variables (refer to **Section S2** in Supplementary Material). The important elements to check the model's reliability and accuracy are the P and F values of the main model. Ideally, P value should be less than 0.5 and the F value greater than 0 for determining the significance of the model for prediction and optimization purposes [24,25]. Other check tests encompass the regression coefficient test (R^2), which should exceed 0.8 for model fitness, and the lack of fitness (LOF) test, which has to be greater than 0.05 for model validation as it is a measure of errors whereby an insignificant lack of fit is desirable for a reliable model [25]. In reference to **Table S2**, the RSM-BBD approach has met all the check

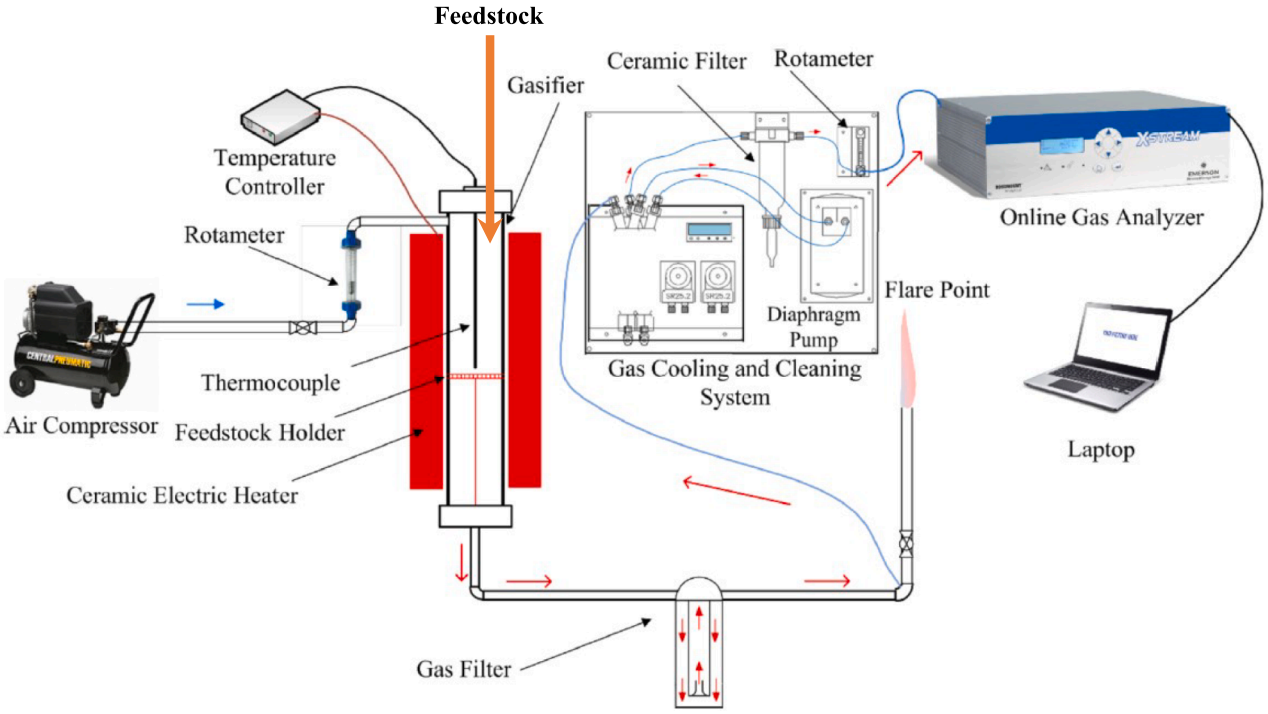

Fig. 1. Schematic diagram of gasification set-up.

Table 3
Parameter span for experiment design using BBD method.

Notation of variables		SI-units	Min.	Max.	Lower-coded	Higher-coded	Mean-value	Std. Dev.
A	Temperature	°C	600	800	−1 ↔ 600	+1 ↔ 800	700	65.47
B	Particle size	mm	2	6	−1 ↔ 2	+1 ↔ 6	4	1.31
C	Catalyst loading	wt.%	0	10	−1 ↔ 0	+1 ↔ 10	5	3.27
D	Air flow rate	L/min	1	3	−1 ↔ 1	+1 ↔ 3	2	0.6547

test requirements and hence indicates that the models are fit and significant.

2.5. Gasification performance

The experimental results attained upon completion of the gasification experiment were evaluated at optimum values. Syngas quality was assessed based on its higher heating value whereas the performance of the gasification process was evaluated in terms of gas yield, cold gas efficiency, and carbon conversion efficiency. The mathematical formulas for each performance indicator can be found under **Section S3** in Supplementary Material.

3. Results and discussion

3.1. Characterization of PKSH catalyst

PKSH is rich in Si (29.6 %), P (14.0 %), Fe (12.5 %), Ca (11.9 %), K (8.39 %), Cl (5.78 %), and S (5.24 %). The presence of basic elements (K, Ca, Mg, Na), amphoteric element (Al), and acidic element (Cl, P, S, and Si) implies that PKSH possesses both basic and acidic active sites which tend to affect the physiochemical properties of the hydrochar. High Si in PKSH suggests that it has many acidic active sites that can presumably intensify the dehydrogenation and hydrocracking reactions [32]. Besides that, the Si/Al value of PKSH is 10.34 which suggests that PKSH is likely to aid in tar cracking reaction during gasification as previous studies had confirmed that low Si/Al value enhances the catalyst acidity which is favorable for cracking reaction [32,33]. FESEM micrograph allows the altered intrinsic properties of the biomass to be observed when PKS is converted to hydrochar via HTC. Fig. 2 **(a)** which shows various irregular pore sizes detected on the coarse surface of the hydrochar reveals there have been loss of volatiles from the hydrochar during HTC. The EDX spectrums in Fig. 2 **(b)** show that PKSH is enriched with C followed by O and other elements such as Cl, K, Ca, Na, Cu, and Mg.

3.2. Combined interaction of parameters on gaseous output from air catalytic gasification of WH using PKSH as catalyst

Table 4 shows the experimental results collected based on the RSM-BBD method which involves the input factors such as temperature (600−800 °C), particle size (2–6 mm), catalyst loading (0–10 wt%) and air flow rate (1–3 L/min) used for the experimental design. The response variables such as H_2, CO, CO_2, and CH_4 are measured from the gas analyzer, allowing the product gas composition to be analyzed.

3.2.1. H_2 composition

The combined interaction effects of the input parameters (temperature, particle size, catalyst loading and air flow rate) on response variable H_2 composition are represented by Fig. 3 **(a, c, e)** in the form of 3D surface and contour plots. It is observed that temperature substantially affects H_2 production as it is a significant factor affecting all stages of devolatilization during the gasification process. Oxidation of char and volatiles, Boudouard reaction and methanation are some examples of the devolatilization reactions mechanisms heavily influenced by temperature [24,26]. These reactions could be exothermic or endothermic depending on their chemical nature which greatly relies on the gasification temperature. According to Le Chatelier's principle, for endothermic reactions to be favored to produce greater H_2 output, high gasification temperatures tend to promote reaction mechanisms such as water-gas shift and primary and secondary water–gas reactions which accelerate H_2 production. Fig. 3 **(a)** demonstrates the combined interaction of temperature and particle size, whereby increasing gasification temperature alongside greater particle size enhanced H_2 production. It was found that the use of smaller particle size, 2 mm, will produce minimal H_2 composition, particularly at low temperature ranges due to low reactivity. The maximum yield of H_2 attained corresponding to the combined interaction is around 11 vol% at 800 °C with particle size of 6 mm. Meanwhile, the collected experimental results in Table 3 show maximum H_2 composition of 11.19 vol% reached at 800 °C with particle size of 4 mm in the absence of catalyst. The combined interaction effects of temperature and catalyst loading are depicted by Fig. 3 **(c).** Increased

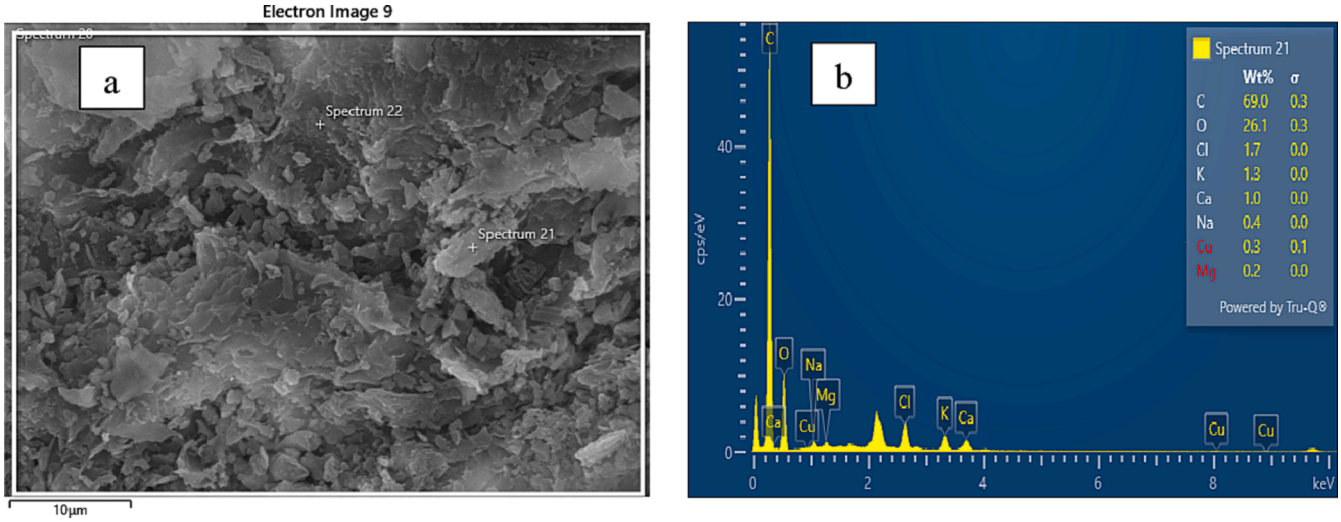

Fig. 2. (a) FESEM (b) EDX spectrum of PKSH.

Table 4
Experimental design using BBD with gaseous output response.

Std	Run	Temperature	Particle size	Catalyst loading	Air flow rate	H_2	CO	CO_2	CH_4
		°C	mm	wt.%	L/min	vol.%	vol.%	vol.%	vol.%
20	1	800	4	10	2	9.55	15.72	24.07	10.5
23	2	700	2	5	3	6.10	8.99	21.65	4.04
2	3	800	2	5	2	6.92	8.82	17.31	6.44
1	4	600	2	5	2	1.91	3.86	12.66	2.05
3	5	600	6	5	2	2.88	6.80	19.92	2.04
26	6	700	4	5	2	7.16	11.75	26.41	5.48
7	7	700	4	0	3	4.10	10.27	18.74	4.68
24	8	700	6	5	3	5.10	11.88	27.81	5.55
22	9	700	6	5	1	7.64	13.25	25.00	8.33
15	10	700	2	10	2	5.31	8.72	17.22	3.20
13	11	700	2	0	2	4.31	7.65	18.19	4.40
14	12	700	6	0	2	7.02	12.24	19.26	4.46
12	13	800	4	5	3	6.19	12.05	17.83	8.33
27	14	700	4	5	2	6.48	10.18	25.71	5.65
16	15	700	6	10	2	7.85	13.01	31.82	11.12
8	16	700	4	10	3	5.50	11.15	25.79	5.69
5	17	700	4	0	1	5.82	9.36	18.54	4.11
10	18	800	4	5	1	10.30	12.27	21.48	9.68
11	19	600	4	5	3	2.88	6.41	19.69	1.90
6	20	700	4	10	1	4.84	8.29	17.97	5.95
17	21	600	4	0	2	2.92	4.59	14.60	4.56
18	22	800	4	0	2	11.19	15.06	20.48	6.63
28	23	700	4	5	2	8.44	9.92	22.06	5.52
9	24	600	4	5	1	2.12	4.30	13.46	3.48
29	25	700	4	5	2	6.22	10.02	22.97	5.41
19	26	600	4	10	2	2.54	6.22	19.14	2.15
25	27	700	4	5	2	6.07	10.78	25.15	5.61
21	28	700	2	5	1	4.77	8.34	17.72	5.18
4	29	800	6	5	2	11.14	18.95	27.59	11.4

H_2 yield is achieved at high temperatures whereas the catalyst loading has a rather marginal effect on the H_2 yield. Nevertheless, Fig. 3 **(c)** shows a slight increase in H_2 composition at 800 °C when catalyst loading was increased to 5 wt% which later has no prominent effect when it was further increased to 10 wt%. Even with high catalyst loading at low temperatures, there was a lack of discernible pattern that shows improvement in the H_2 yield. The slight increase in H_2 output may be attributed to the catalytic effect of inorganic elements in PKSH such as K, Ca and Fe which enhanced the H_2 production [34]. In terms of the combined interaction of temperature and air flow rate, Fig. 3 **(e)** portrays a noteworthy observation on high H_2 output achieved with lower air flow rate at higher temperature range. A similar observation on the effect of air flow rate was also reported in the study by Ali et al. 2022 [24]. The inverse effect of air flow rate on H_2 production could be due to favored oxidation reactions to produce CO. The order of influencing factors on H_2 production for the present study would be temperature > particle size > air flow rate > catalyst loading.

3.2.2. *CO composition*

The combined interaction effects of the input parameters (temperature, particle size, catalyst loading and air flow rate) on response variable CO composition are represented by Fig. 3 **(b, d, f)** in the form of 3D surface and contour plots. Fig. 3 **(b)** shows the combined interaction of temperature and particle size. For the same particle size of 2 mm, the effect of temperature on the CO yield is not as apparent when compared to the bigger particle size used. In this case, particle size plays a crucial role in achieving greater CO yield. Maximum CO yield of 18.95 vol% was achieved with particle size of 6 mm at 800 °C. Fig. 3 **(d)** shows the combined interaction effect of temperature and catalyst loading. Catalyst loading appears to have relatively less impact on CO yield compared to temperature as the increment of catalyst loading does not bring about significant impact on the CO yield at each temperature point. Fig. 3 **(f)** shows the combined interaction effect of temperature and air flow rate. Likewise, the dual parameters exhibit mutual interaction as the previous pair of parameters as demonstrated in Fig. 3 **(d)** though there is a slightly more evident change in CO yield at each temperature. A slight increase in CO yield can be observed when the air flow rate is configured to 2–2.5 L/min. Increasing the air flow rate at high temperatures could enhance the oxidation reaction while inhibiting the steam gasification reaction, thereby increasing the production of CO gas [24]. The order of influencing factors on CO output is similar to that of the H_2 output.

3.2.3. *CO_2 composition*

The combined interaction effects of the input parameters (temperature, particle size, catalyst loading and air flow rate) on response variable CO_2 composition are represented by Fig. 4 **(a, c, e)** in the form of 3D surface and contour plots. Fig. 4 **(a)** shows the combined interaction effect of temperature and particle size. In this case, particle size has a greater impact on CO_2 yield compared to temperature. Higher yield was achieved when temperature was raised from 600 °C to 700 °C and further increasing the temperature led to decreased CO_2 yield. Meanwhile, a larger particle size of 6 mm will result in higher CO_2 yield, particularly at temperatures around 700–750 °C. Fig. 4 **(c)** shows the combined interaction effect of temperature and catalyst loading while Fig. 4 **(e)** shows the effect of temperature and air flow rate. Both pairs of dual parameters exhibit a hyperbola trend. It can be observed that a temperature of 700–750 °C is again the desirable temperature for higher CO_2 output. According to Fig. 4 **(e)**, higher CO_2 is achievable with 24 vol % CO_2 yield at higher catalyst loading and air flow rate of 2 L/min. This is because PKSH is rich in C while increasing the air flow rate will promote oxidation reaction, thus leading to greater CO_2 output [24,35]. The order of influencing factors on CO_2 production for the present study is particle size > temperature > air flow rate > catalyst loading.

3.2.4. *CH_4 composition*

The combined interaction effects of the input parameters (temperature, particle size, catalyst loading and air flow rate) on response variable CH_4 composition are represented by Fig. 4 **(b, d, f)** in the form of 3D surface and contour plots. Fig. 4 **(b)** shows the combined interaction effect of temperature and particle size whereas Fig. 4 **(d)** shows the

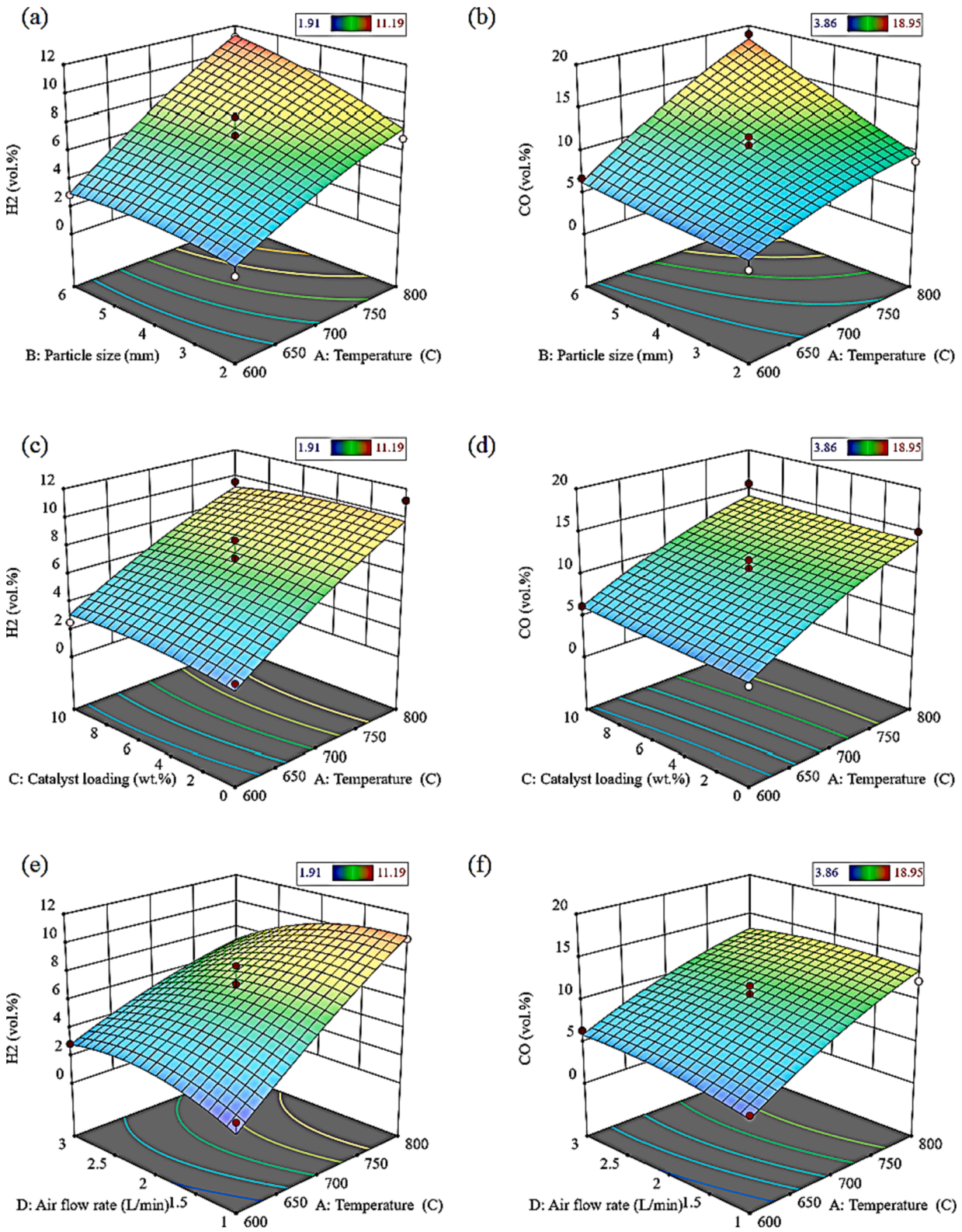

Fig. 3. 3D surface and contour plots of H_2 and CO composition (vol.%) from catalytic conversion of WH using PKSH as catalyst in the form of combined interactions of (a, b) temperature (600–800 °C) and particle size (2–6 mm), (b, c) temperature and catalyst loading (0-10 wt%) and (e, f) temperature and air flow rate (1–3 L/min).

combined interaction effect of temperature and catalyst loading. Both figures show a similar trend whereby temperature does not seem to be of great influence on CH_4 output with smaller particle size and lower catalyst loading. The effect of temperature is more evident when gasifying larger range particle sizes were used as the CH_4 gas reached a maximum yield of 11.4 vol% at 800 °C at higher catalyst loading. With smaller particle size, a greater surface area exists for better heat transfer and hence reducing the methanation reaction, giving low CH_4 output

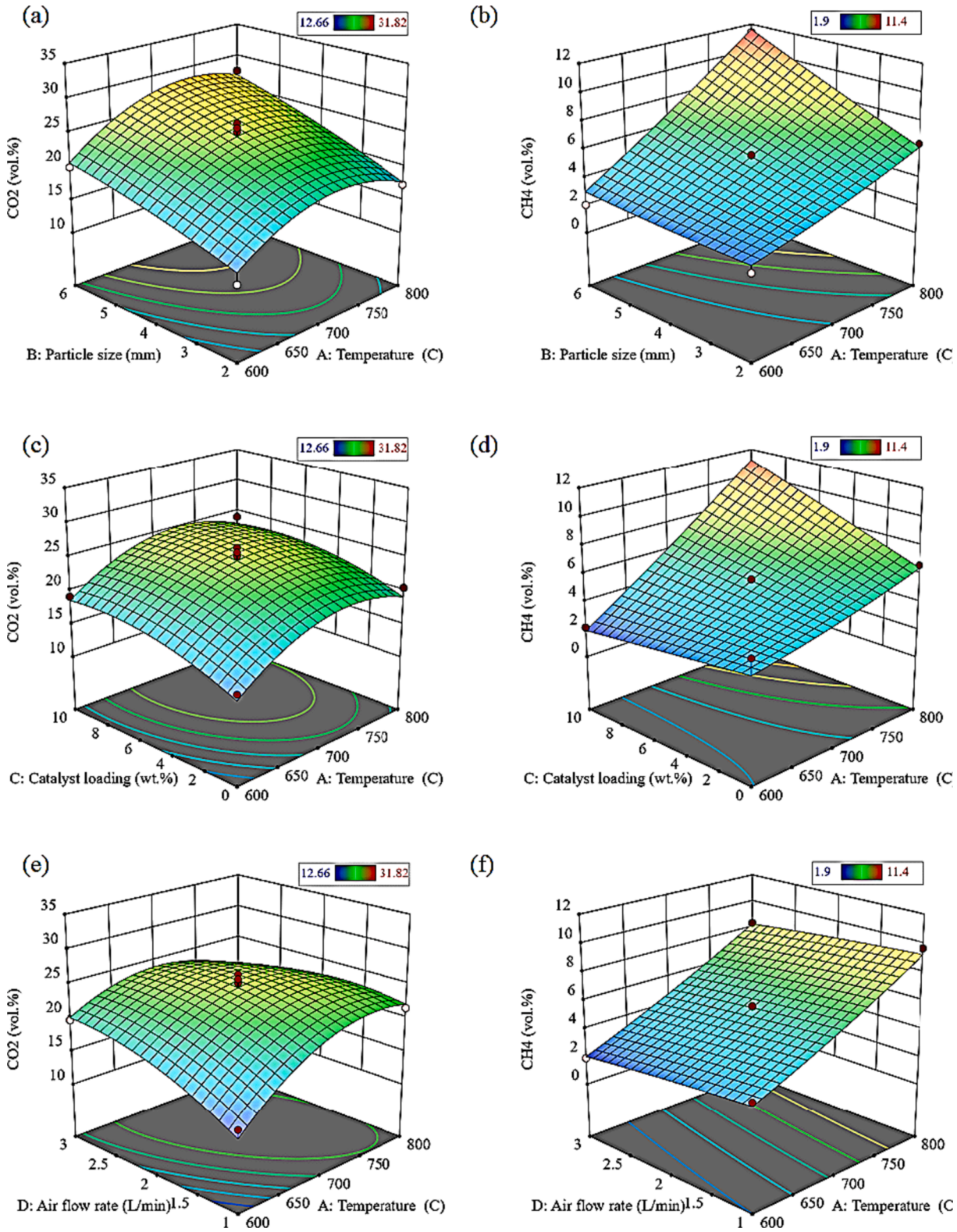

Fig. 4. 3D surface and contour plots of CO_2 and CH_4 composition (vol.%) from catalytic conversion of WH using PKSH as catalyst in the form of combined interactions of (a, b) temperature (600-800°C) and particle size (2–6 mm), (c, d) temperature and catalyst loading (0-10 wt%) and (e, f) temperature and air flow rate (1–3 L/min).

[24]. Fig. 4 **(f)** shows the combined interaction effect of temperature and air flow rate. CH_4 output increases at a lower air flow rate when temperature is increased. Further increasing the air flow rate results in lower CH_4 production. It is presumed that low temperature and air flow rate will promote methanation reaction and thereby leading to high CH_4 output [24]. The order of influencing factors on CH_4 output be arranged as temperature > particle size > catalyst loading > air flow rate.

3.3. Influence of PKSH on gasification performance

The gasification performance can be assessed based on several indicators such as the gas yield, syngas heating value, carbon conversion efficiency (CCE) and cold gas efficiency (CGE). These parameters help to define the capability of the gasification process in terms of its viability, quality and economy [36]. According to Fig. 5, gasification temperature exhibits a direct relationship with the syngas heating value, gas yield, CCE and CGE. For comparison of the effect of temperature and catalyst loading, the air flow rate and biomass particle size are kept constant at 2 L/min and 4 mm, respectively. When the temperature was increased from 600 to 800 °C, under non-catalytic conditions, syngas yield was increased from 7.51 to 26.25 vol% and syngas heating value was increased from 2.77 to 5.97 MJ/Nm^3. At 800 °C, addition of 5 wt% PKSH catalyst has increased the syngas yield to 33.09 vol% and caused a huge jump in the gasification performance parameters as portrayed by Fig. 5 **(b)**. Temperature deemed as the governing factor has given rise to the optimum performance of the PKSH catalyst with remarkably high gasification performance such as syngas heating value of 11.16 MJ/Nm^3, gas yield of 1.65 Nm^3/kg, CCE and CGE of 191.36 % and 121.40 %, respectively. Further increment to 10 wt% PKSH at 800 °C did not increase the gasification performance, with calculated syngas heating value, gas yield, CCE, and CGE of 8.35 MJ/Nm^3, 1.02 Nm^3/kg, 98.90 % and 56.02 %, respectively.

3.4. Role of PKSH catalyst

According to the characterization results, the presence of inorganic elements such as Fe, Ca and K and the porous surface of the hydrochar acting as active sites are believed to have enhanced the gasification process. It can be deduced that the evolution of the pores may have been influenced by the formation of mineral oxides such as CaO and K_2O, which suggests increased gasification reactivity. This leads to the apparent increase in gas yield, HHV, CCE, and CGE as shown by Fig. 5 **(b)**. Studies conducted by Gai et al. and Feng et al. have reported on the enhanced gas yield and gasification efficiency involving hydrochar catalysts due to the presence of inorganic elements such as AAEMs (i.e., K, Ca) on the surface of hydrochar [37–39]. Theoretically, Fe found in PKSH can be integrally allied with the carboxyl functional groups present in biomass. These carboxyl groups may have disintegrated to form Fe_2O_3 during gasification reaction which supports the syngas genesis [34]. The presence of Fe_2O_3 further induces catalytic effect on the gasification process such that:

$$CO + FeO \leftrightarrow CO_2 + Fe \quad (1)$$

$$C + Fe \leftrightarrow CO + Fe \quad (2)$$

Study conducted by Feng et al. have proposed a catalytic mechanism of K-O-C group formation as an active site on the biochar structure during gasification [39]. It is deduced that an intermediate C_nK is formed and exists between the carbon layers when K reacts with the aromatic rings [40]. The presence of AAEMs in the PKSH may have exhibited a similar mechanism during gasification whereby the AAEMs linked to the carbon matrix migrate to the gas–solid interface. This leads to bond breaking and forming, resulting in the condensation of aromatic rings as well as the generation and regeneration of porous structures on the hydrochar surface, giving rise to the formation of active sites to catalyze the gasification process while reducing tar formation.

4. Conclusion

The conversion of WH biomass into syngas-enriched hydrogen via air gasification process was carried out in a lab-scale downdraft gasifier. Air as the selected gasifying agent for the present study reveals its potential as an economically viable process alongside ease of operation to produce a decent amount of H_2 on a small and medium scale. The experimental design adopted the RSM-BBD method for the parametric study which involves several operating parameters such as temperature (600–800 °C), biomass particle size (2–6 mm), catalyst loading (0–10 wt %), and air flow rate (1–3 L/min). It was deduced that temperature presents the most influential effect on the gaseous output. Maximum syngas (H_2 + CO) of 30.09 vol% was attained at 800 °C with a particle size of 6 mm and air flow rate of 2 L/min alongside 5 wt% PKSH. The influencing order for H_2 output is temperature > particle size > air flow rate > catalyst loading. Based on the gasification performance indicators, favorable results were obtained with syngas heating value of 11.16 MJ/Nm^3, gas yield of 1.65 Nm^3/kg, CCE of 191.36 %, and CGE 121.40 %.

CRediT authorship contribution statement

April Ling Kwang Chee: Writing – original draft, Validation, Software, Investigation, Formal analysis, Data curation, Conceptualization, Writing – review & editing, Methodology, Visualization. **Bridgid Lai Fui Chin:** Writing – review & editing, Supervision, Resources, Project administration, Funding acquisition, Formal analysis, Conceptualization, Investigation, Methodology, Validation. **Shaharin Anwar Sulaiman:** Writing – review & editing, Supervision, Resources, Methodology, Formal analysis, Conceptualization, Investigation, Validation. **Yee Ho Chai:** Writing – review & editing, Supervision, Resources, Methodology, Formal analysis, Conceptualization, Investigation, Validation. **Agus Saptoro:** Writing – review & editing, Supervision, Methodology, Formal analysis, Investigation, Validation. **Hadiza Aminu Umar:** Resources, Formal analysis. **Serene Sow Mun Lock:** Writing – review & editing, Investigation. **Chung Long Yiin:** Writing – review & editing, Investigation.

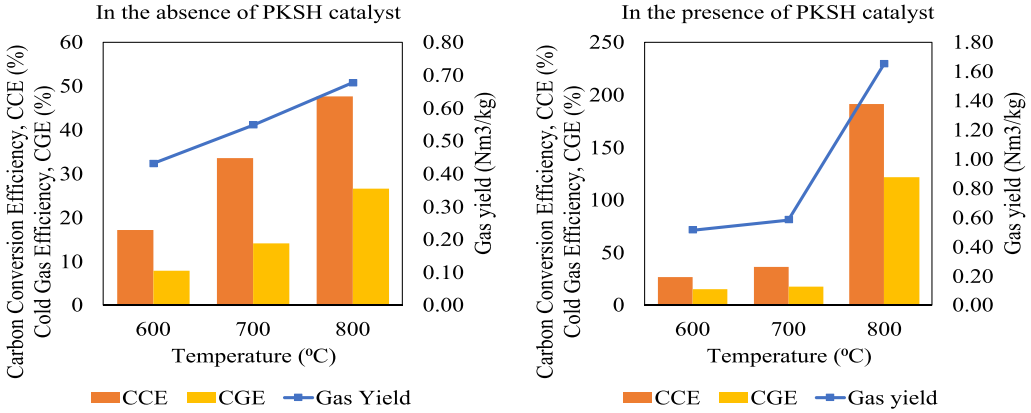

Fig. 5. Effect of PKSH on gasification performance (a) in the absence of PKSH catalyst, (b) in the presence of PKSH catalyst.

Declaration of competing interest

The authors declare that they have no known competing financial interests or personal relationships that could have appeared to influence the work reported in this paper.

Data availability

Data will be made available on request.

Acknowledgments

The authors fully appreciate the financial support and facilities under the Curtin Malaysia Sustainability Research Grant 2021 on the research project entitled, 'Conversion of water hyacinth to syngas enriched hydrogen production via catalytic gasification process'. And also, the authors would like to thank Curtin University Malaysia for providing the Curtin Malaysia Postgraduate Research Scholarship (CMPRS) to the first author and contributing the necessary resources for this project. Special gratitude is also expressed towards the Biomass Processing Laboratory, Centre of Biofuel and Biochemical (CBBR) of Universiti Teknologi PETRONAS (UTP) and Curtin University Malaysia for their technical supports.

Appendix A. Supplementary data

Supplementary data to this article can be found online at https://doi.org/10.1016/j.fuel.2023.130811.

References

[1] Chee ALK, Chin BLF, Goh SMX, Chai YH, Loy ACM, Cheah KW, et al. Thermo-catalytic co-pyrolysis of palm kernel shell and plastic waste mixtures using bifunctional HZSM-5/limestone catalyst: Kinetic and thermodynamic insights. J Energy Inst 2023;107:101194. https://doi.org/10.1016/j.joei.2023.101194.
[2] Yap TL, Loy ACM, Chin BLF, Lim JY, Alhamzi H, Chai YH, et al. Synergistic effects of catalytic co-pyrolysis Chlorella vulgaris and polyethylene mixtures using artificial neuron network: Thermodynamic and empirical kinetic analyses. J Environ Chem Eng 2022;10(3):107391. https://doi.org/10.1016/j.jece.2022.107391.
[3] Chin BLF, Gorin A, Chua HB, Twaiq F. Experimental investigation on tar produced from palm shells derived syngas using zeolite HZSM-5 catalyst. J Energy Institute 2016;89(4):713–24. https://doi.org/10.1016/j.joei.2015.04.005.
[4] Materazzi M. Gasification of Waste Derived Fuels in Fluidized Beds: Fundamental Aspects and Industrial. Challenges 2017:19–63. https://doi.org/10.1007/978-3-319-46870-9_2.
[5] Zhao M, Raheem A, Memon ZM, Vuppaladadiyam AK, Ji G. Iso-conversional kinetics of low-lipid micro-algae gasification by air. J Clean Prod 2019;207:618–29. https://doi.org/10.1016/j.jclepro.2018.10.040.
[6] Li M, Zhang YS, Cheng S, Qu B, Li A, Meng F, et al. The impact of heating rate on the decomposition kinetics and product distribution of algal waste pyrolysis with in-situ weight measurement. Chem Eng J 2023;457:141368. https://doi.org/10.1016/j.cej.2023.141368.
[7] Wauton I, Ogbeide SE. Investigation of the production of pyrolytic bio- oil from water hyacinth (Eichhornia crassipes) in a fixed bed reactor using pyrolysis process. Biofuels 2019:1–7. https://doi.org/10.1080/17597269.2019.1660061.
[8] Tran TK, Kim N, Leu HJ, Pham MP, Luong NA, Vo HK. The production of hydrogen gas from modified water hyacinth (Eichhornia Crassipes) biomass through pyrolysis process. Int J Hydrog Energy 2021;46:13976–84. https://doi.org/10.1016/j.ijhydene.2020.08.225.
[9] Bhattacharjee N, Biswas AB. Value-added fuels from the catalytic pyrolysis of Alternanthera philoxeroides. Fuel 2021;295:120629. https://doi.org/10.1016/j.fuel.2021.120629.
[10] Rahman MA. Pyrolysis of water hyacinth in a fixed bed reactor: Parametric effects on product distribution, characterization and syngas evolutionary behavior. Waste Manag 2018;80:310–8. https://doi.org/10.1016/j.wasman.2018.09.028.
[11] Zhong S, Zhang B, Liu C, Shujaa AA. Mechanism of synergistic effects and kinetics analysis in catalytic co-pyrolysis of water hyacinth and HDPE. Energy Convers Manag 2021;228:113717. https://doi.org/10.1016/j.enconman.2020.113717.
[12] Azwar E, Wan Mahari WA, Rastegari H, Tabatabaei M, Peng W, Tsang YF, et al. Progress in thermochemical conversion of aquatic weeds in shellfish aquaculture for biofuel generation: Technical and economic perspectives. Bioresour Technol 2022;344:126202. https://doi.org/10.1016/j.biortech.2021.126202.
[13] Bronzato GRF, Ziegler SM, Silva RC, Cesarino I, Leão AL. Characterization of the pre-treated biomass of Eichhornia crassipes (water hyacinth) for the second generation ethanol production. Mol Cryst Liq Cryst 2017;655:224–35. https://doi.org/10.1080/15421406.2017.1360696.
[14] Hu Z, Ma X, Li L. Optimal conditions for the catalytic and non-catalytic pyrolysis of water hyacinth. Energy Convers Manag 2015;94:337–44. https://doi.org/10.1016/j.enconman.2015.01.087.
[15] Huang H, Liu J, Liu H, Evrendilek F, Buyukada M. Pyrolysis of water hyacinth biomass parts: Bioenergy, gas emissions, and by-products using TG-FTIR and Py-GC/MS analyses. Energy Convers Manag 2020;207:112552. https://doi.org/10.1016/j.enconman.2020.112552.
[16] Matsumura Y. Evaluation of supercritical water gasification and biomethanation for wet biomass utilization in Japan. Energy Convers Manag 2002;43:1301–10. https://doi.org/10.1016/S0196-8904(02)00016-X.
[17] Pereira Lopes R, Astruc D. Biochar as a support for nanocatalysts and other reagents: Recent advances and applications. Coord Chem Rev 2021;426:213585. https://doi.org/10.1016/j.ccr.2020.213585.
[18] Buentello-Montoya D, Zhang X, Li J, Ranade V, Marques S, Geron M. Performance of biochar as a catalyst for tar steam reforming: Effect of the porous structure. Appl Energy 2020;259. https://doi.org/10.1016/j.apenergy.2019.114176.
[19] Kang K, Nanda S, Hu Y. Current trends in biochar application for catalytic conversion of biomass to biofuels. Catal Today 2022;404:3–18. https://doi.org/10.1016/j.cattod.2022.06.033.
[20] Gai C, Zhang F, Yang T, Liu Z, Jiao W, Peng N, et al. Hydrochar supported bimetallic Ni–Fe nanocatalysts with tailored composition, size and shape for improved biomass steam reforming performance. Green Chem 2018;20:2788–800. https://doi.org/10.1039/C8GC00433A.
[21] Gai C, Zhang F, Guo Y, Peng N, Liu T, Lang Q, et al. Hydrochar-supported, in situ-generated nickel nanoparticles for sorption-enhanced catalytic gasification of sewage sludge. ACS Sustain Chem Eng 2017:5. https://doi.org/10.1021/acssuschemeng.7b00924.
[22] Ren J, Cao J-P, Zhao X-Y, Yang F-L, Wei X-Y. Recent advances in syngas production from biomass catalytic gasification: A critical review on reactors, catalysts, catalytic mechanisms and mathematical models. Renew Sustain Energy Rev 2019;116:109426. https://doi.org/10.1016/j.rser.2019.109426.
[23] Dahou T, Defoort F, Khiari B, Labaki M, Dupont C, Jeguirim M. Role of inorganics on the biomass char gasification reactivity: A review involving reaction mechanisms and kinetics models. Renew Sustain Energy Rev 2021;135:110136. https://doi.org/10.1016/j.rser.2020.110136.
[24] Ali AM, Inayat M, Zahrani AA, Shahzad K, Shahbaz M, Sulaiman SA, et al. Process optimization and economic evaluation of air gasification of Saudi Arabian date palm fronds for H2-rich syngas using response surface methodology. Fuel 2022;316:123359. https://doi.org/10.1016/j.fuel.2022.123359.
[25] Umar HA, Sulaiman SA. Parametric optimisation through the use of Box-Behnken design in the Co-gasification of oil palm trunk and frond for syngas production. Fuel 2022;310:122234. https://doi.org/10.1016/j.fuel.2021.122234.
[26] Inayat M, Sulaiman SA, Inayat A, Shaik NB, Gilal AR, Shahbaz M. Modeling and parametric optimization of air catalytic co-gasification of wood-oil palm fronds blend for clean syngas (H2+CO) production. Int J Hydrog Energy 2021;46:30559–80. https://doi.org/10.1016/j.ijhydene.2020.10.268.
[27] Sarker TR, Nanda S, Dalai AK. Parametric studies on hydrothermal gasification of biomass pellets using Box-Behnken experimental design to produce fuel gas and hydrochar. J Clean Prod 2023;388:135804. https://doi.org/10.1016/j.jclepro.2022.135804.
[28] Umar HA, Sulaiman SA, Said MA, Gungor A, Ahmad RK, Inayat M. Syngas production from gasification and co-gasification of oil palm trunk and frond using a down-draft gasifier. Int J Energy Res 2021;45:8103–15. https://doi.org/10.1002/er.6345.
[29] Fagernäs L, Brammer J, Wilén C, Lauer M, Verhoeff F. Drying of biomass for second generation synfuel production. Biomass Bioenergy 2010;34:1267–77. https://doi.org/10.1016/j.biombioe.2010.04.005.
[30] Chen W-H, Peng J, Bi XT. A state-of-the-art review of biomass torrefaction, densification and applications. Renew Sustain Energy Rev 2015;44:847–66. https://doi.org/10.1016/j.rser.2014.12.039.
[31] Lui J, Chen W-H, Tsang DCW, You S. A critical review on the principles, applications, and challenges of waste-to-hydrogen technologies. Renew Sustain Energy Rev 2020;134:110365. https://doi.org/10.1016/j.rser.2020.110365.
[32] Loy ACM, Yusup S, Lam MK, Chin BLF, Shahbaz M, Yamamoto A, et al. The effect of industrial waste coal bottom ash as catalyst in catalytic pyrolysis of rice husk for syngas production. Energy Convers Manag 2018;165:541–54. https://doi.org/10.1016/j.enconman.2018.03.063.
[33] Chen G-Y, Liu C, Ma W-C, Yan B-B, Ji N. Catalytic Cracking of Tar from Biomass Gasification over a HZSM-5-Supported Ni–MgO Catalyst. Energy Fuels 2015;29:7969–74. https://doi.org/10.1021/acs.energyfuels.5b00830.
[34] Kamble AD, Mendhe VA, Chavan PD, Saxena VK. Insights of mineral catalytic effects of high ash coal on carbon conversion in fluidized bed Co-gasification through FTIR, XRD. XRF and FE-SEM Renew Energy 2022;183:729–51. https://doi.org/10.1016/j.renene.2021.11.022.
[35] Yusup S, Khan Z, Ahmad MM, Rashidi NA. Optimization of hydrogen production in in-situ catalytic adsorption (ICA) steam gasification based on Response Surface Methodology. Biomass Bioenergy 2014;60:98–107. https://doi.org/10.1016/j.biombioe.2013.11.007.
[36] Shahbaz M, Al-Ansari T, Inayat M, Sulaiman SA, Parthasarathy P, McKay G. A critical review on the influence of process parameters in catalytic co-gasification: Current performance and challenges for a future prospectus. Renew Sustain Energy Rev 2020;134:110382. https://doi.org/10.1016/j.rser.2020.110382.
[37] Gai C, Guo Y, Liu T, Peng N, Liu Z. Hydrogen-rich gas production by steam gasification of hydrochar derived from sewage sludge. Int J Hydrog Energy 2016;41:3363–72. https://doi.org/10.1016/j.ijhydene.2015.12.188.

[38] Gai C, Chen M, Liu T, Peng N, Liu Z. Gasification characteristics of hydrochar and pyrochar derived from sewage sludge. Energy 2016;113:957–65. https://doi.org/10.1016/j.energy.2016.07.129.
[39] Feng D, Zhao Y, Zhang Y, Xu H, Zhang L, Sun S. Catalytic mechanism of ion-exchanging alkali and alkaline earth metallic species on biochar reactivity during CO2/H2O gasification. Fuel 2018;212:523–32. https://doi.org/10.1016/j.fuel.2017.10.045.
[40] Wang X, Chen Q, Zhu H, Chen X, Yu G. In-situ study on structure evolution and gasification reactivity of biomass char with K and Ca catalysts at carbon dioxide atmosphere. Carbon Resour Convers 2023;6:27–33. https://doi.org/10.1016/j.crcon.2022.10.002.